Radiology

Deep Learning for Diagnosis of Chronic Myocardial Infarction on Nonenhanced Cardiac Cine MRI

*Nan Zhang, MD** • *Guang Yang, MSc, PhD** • *Zhifan Gao, PhD* • *Chenchu Xu, PhD* • *Yanping Zhang, PhD* • *Rui Shi, MD, PhD* • *Jennifer Keegan, PhD* • *Lei Xu, MD* • *Heye Zhang, PhD* • *Zhanming Fan, MD* • *David Firmin, PhD*

From the Department of Radiology, Beijing Anzhen Hospital, Capital Medical University, 2nd Anzhen Road, Chaoyang District, Beijing, China (N.Z., L.X., Z.F.); Cardiovascular Research Centre, Royal Brompton Hospital, London, England (G.Y., R.S., J.K., D.F.); National Heart and Lung Institute, Imperial College London, London, England (G.Y., R.S., J.K., D.F.); Shenzhen Institutes of Advanced Technology, Chinese Academy of Sciences, Shenzhen, China (Z.G., H.Z.); Anhui University, Hefei, China (C.X., Y.Z.); and School of Biomedical Engineering, Sun Yat-Sen University, Shenzhen, China (H.Z.). Received October 8, 2018; revision requested November 15; revision received March 4, 2019; accepted March 14. **Address correspondence to** L.X. (e-mail: *leixu2001@hotmail.com*).

N.Z. and L.X. supported by National Key Research and Development Program of China (2016YFC1300300). N.Z. and L.X. also supported by National Natural Science Foundation of China (No. 81641069). H.Z. supported by National Natural Science Foundation of China (No. U1801265, 61525106, and 6771464). G.Y., J.K., and D.F. supported by British Heart Foundation (PG/16/78/32402).

*N.Z. and G.Y. contributed equally to this work.

Conflicts of interest are listed at the end of this article.

See also the editorial by Leiner in this issue.

Radiology 2019; 291:606–617 • https://doi.org/10.1148/radiol.2019182304 • Content codes: CA MR

Background: Renal impairment is common in patients with coronary artery disease and, if severe, late gadolinium enhancement (LGE) imaging for myocardial infarction (MI) evaluation cannot be performed.

Purpose: To develop a fully automatic framework for chronic MI delineation via deep learning on non–contrast material–enhanced cardiac cine MRI.

Materials and Methods: In this retrospective single-center study, a deep learning model was developed to extract motion features from the left ventricle and delineate MI regions on nonenhanced cardiac cine MRI collected between October 2015 and March 2017. Patients with chronic MI, as well as healthy control patients, had both nonenhanced cardiac cine (25 phases per cardiac cycle) and LGE MRI examinations. Eighty percent of MRI examinations were used for the training data set and 20% for the independent testing data set. Chronic MI regions on LGE MRI were defined as ground truth. Diagnostic performance was assessed by analysis of the area under the receiver operating characteristic curve (AUC). MI area and MI area percentage from nonenhanced cardiac cine and LGE MRI were compared by using the Pearson correlation, paired *t* test, and Bland-Altman analysis.

Results: Study participants included 212 patients with chronic MI (men, 171; age, 57.2 years ± 12.5) and 87 healthy control patients (men, 42; age, 43.3 years ± 15.5). Using the full cardiac cine MRI, the per-segment sensitivity and specificity for detecting chronic MI in the independent test set was 89.8% and 99.1%, respectively, with an AUC of 0.94. There were no differences between nonenhanced cardiac cine and LGE MRI analyses in number of MI segments (114 vs 127, respectively; $P = .38$), per-patient MI area (6.2 cm^2 ± 2.8 vs 5.5 cm^2 ± 2.3, respectively; $P = .27$; correlation coefficient, $r = 0.88$), and MI area percentage (21.5% ± 17.3 vs 18.5% ± 15.4; $P = .17$; correlation coefficient, $r = 0.89$).

Conclusion: The proposed deep learning framework on nonenhanced cardiac cine MRI enables the confirmation (presence), detection (position), and delineation (transmurality and size) of chronic myocardial infarction. However, future larger-scale multicenter studies are required for a full validation.

Online supplemental material is available for this article.

Diagnosis of chronic myocardial infarction (MI) is an important clinical task because the management of and treatment planning for patients is different for chronic MI versus acute MI (1,2). The extent of chronic MI, including location, size, and transmurality, provides rich information for patient diagnosis, prognosis, and therapy planning (3). Therefore, accurate delineation and comprehensive evaluation of chronic MI is of great clinical interest.

Late gadolinium enhancement (LGE) MRI has been established as the ground truth reference technique for chronic MI evaluation (4–6). However, including LGE MRI in the MRI examination extends the scanning duration and there are also growing concerns about its safety (7–9). While LGE MRI is contraindicated in patients with severe renal impairment, a recent study has also shown that gadolinium might deposit into the skin, dentate nucleus, and globus pallidus of patients with normal renal function (10). A reliable technique to detect and delineate MI without the need for gadolinium-based contrast agent would therefore be highly desirable.

T1 and T2 mapping techniques (11) are non–contrast material–enhanced approaches that show longer T1 and T2 relaxation times in acute MI compared with normal myocardium. In comparison, while T1 relaxation time is

Abbreviations

AUC = area under the receiver operating characteristic curve, CI = confidence interval, LGE = late gadolinium enhancement, MI = myocardial infarction

Summary

Deep learning on nonenhanced cardiac MRI data can detect the presence and extent of chronic myocardial infarction. This approach may have potential to reduce use of gadolinium contrast administration.

Key Points

- A deep learning method to identify myocardial infarction on nonenhanced cardiac cine MRI achieved good diagnostic performance for detecting chronic myocardial infarction (per-segment sensitivity, 90%; specificity, 99%; area under the receiver operating characteristic curve, 0.94).
- There was no difference between the area of chronic MI detected on nonenhanced cardiac cine MRI and ground truth defined by expert manual segmentation of late gadolinium enhancement MRI (per-patient myocardial infarction area, 6.2 cm^2 ± 2.8 vs 5.5 cm^2 ± 2.3, respectively; P = .27).

longer in chronic MI than in normal myocardium, resolution of edema within the infarct results in no significant difference in T2 (8,12,13). However, while reproducible (8,14), measured relaxation times are protocol and field-strength specific and normal ranges are broad (15–17). These techniques also require the acquisition of additional multiple breath-hold data sets with appropriate MRI sequences and extend overall examination duration. Alternatively, MRI feature tracking is an approach that differentiates regional myocardial morphology and cardiac wall motion abnormalities resulting from MI (18,19) on non–contrast-enhanced cardiac cine MRI, which is acquired as part of a standard cardiac MRI examination. However, only the presence and position information of the MI can be extracted from these examinations and these techniques may be further limited by the need for time-consuming processing after the examination.

We propose a fully automatic framework for chronic MI delineation via deep learning on nonenhanced cardiac cine MRI and assess its accuracy for identifying the presence, position, transmurality, and size of the MI without the need for gadolinium injection.

Materials and Methods

This retrospective study was approved by our institutional review board in accordance with local ethics procedures. Further consent was waived with approval.

Patients

Detailed demographics and left ventricle volumetric data are summarized in Table 1. Between October 2015 and March 2017, 212 patients with chronic MI (based on clinical symptoms, electrocardiogram changes, and greater than twofold elevation of creatine kinase and/or positive troponin T) and 87 control patients (without negative LGE MRI) were selected from a single center for retrospective inclusion in our study (Fig 1, Appendix E1 [online]). Major exclusion criteria were acute MI, angina without MI, all kinds of nonischemic cardiomyopathy, cardiac neoplasm, valvular heart disease, congenital

Table 1: Demographics of Patients and Control Patients with Left Ventricle Volumetric Data

	Training			Independent Testing		
Characteristic	Patients with Chronic MI (n = 169)	Control Patients (n = 69)	P Value	Patients with Chronic MI (n = 43)	Control Patients (n = 18)	P Value
Male patient	131 (77.5)	33 (47.8)	.001	40 (93.0)	9 (50.0)	.001
Age (y)*	59.8 ± 11.1	46.4 ± 15.3	<.001	56.8 ± 11.0	40.1 ± 13.5	<.001
Weight (kg)*	76.6 ± 12.3	77.8 ± 24.1	.82	74.2 ± 12.0	70.7 ± 8.8	.26
Height (cm)*	169.2 ± 6.1	165.1 ± 15.3	.23	170.0 ± 7.0	167.6 ± 8.3	.58
Left ventricular ejection fraction (%)*	34.1 ± 17.8	60.8 ± 8.4	<.001	38.0 ± 18.4	58.6 ± 8.0	<.001
Left ventricular end-diastolic volume index (mL/m^2)*	155.3 ± 89.0	89.0 ± 18.3	<.001	132.6 ± 68.0	90.2 ± 20.2	.001
Left ventricular end-systolic volume index (mL/m^2)*	112.9 ± 88.9	36.6 ± 19.5	<.001	88.9 ± 71.2	35.4 ± 13.5	<.001
Stroke volume (mL)*	43.9 ± 20.6	57.8 ± 13.3	<.001	41.2 ± 14.8	58.5 ± 13.8	<.001
Cardiac output (L/min)*	3.5 ± 2.5	4.4 ± 1.4	.002	3.2 ± 1.5	4.2 ± 1.2	.001
Coronary risk factors						
Hypertension	86 (50.9)	19 (27.5)	.001	18 (41.9)	5 (27.8)	.31
Diabetes	60 (35.5)	15 (21.7)	.03	13 (30.2)	3 (16.7)	.28
Smoking	98 (58.0)	22 (31.9)	<.001	17 (39.5)	3 (16.7)	.09
Dyslipidemia	43 (25.4)	5 (7.2)	.001	17 (39.5)	4 (22.2)	.20
Family history	11 (6.5)	4 (5.8)	.84	2 (4.7)	2 (11.1)	.36

Note.—Unless otherwise indicated, data are medians. Data in parentheses are percentages. Independent t tests were used to compare the differences between two groups for continuous numerical variables. χ^2 tests were used to compare the differences between two groups for sex and coronary risk factors. MI = myocardial infarction.

* Data are mean ± SD.

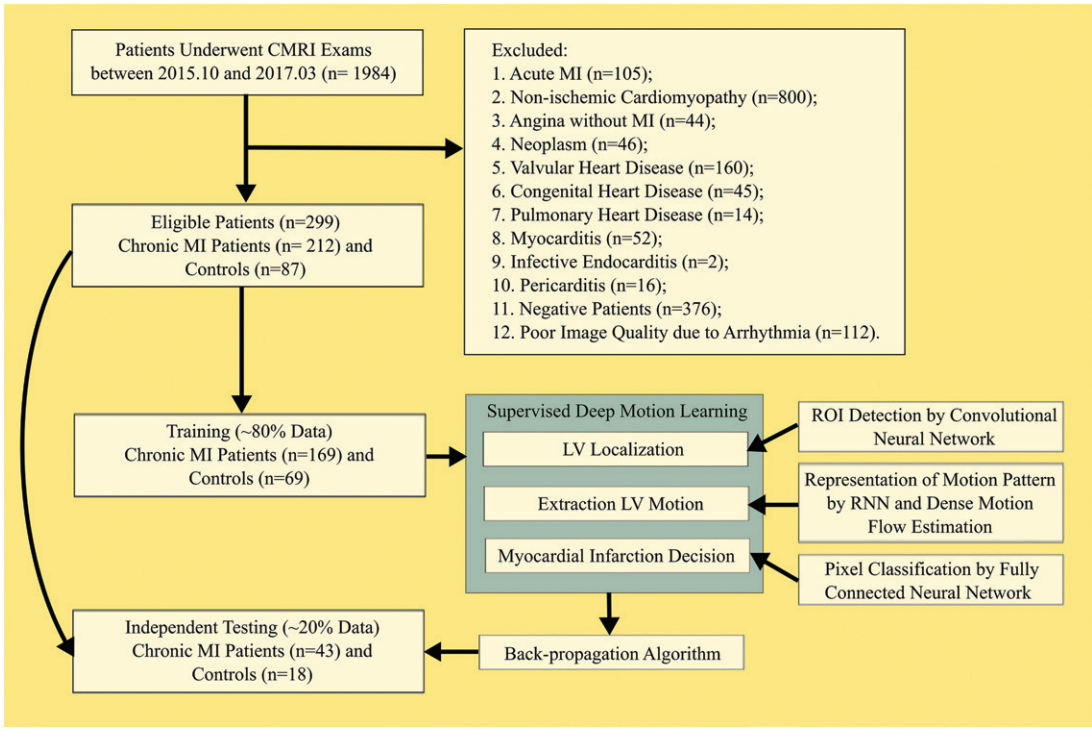

Figure 1: Flow diagram shows the selection and analysis of patients with chronic myocardial infarction (MI) (*n* = 212) and control patients (*n* = 87), the latter being randomly selected from 376 patients scanned between 2015 and 2017 with negative late gadolinium enhancement (LGE) MRI results. In the training data set (80% of study participants), a supervised deep learning framework was developed to locate the left ventricle (LV), to explore local and global motion patterns, and to compare with regions of MI manually outlined in LGE MRI. Predictive performance of the deep learning was assessed by using a further independent testing data set (20% of study participants). CMRI = cardiac MRI, ROI = region of interest, RNN = recurrent neural network.

heart disease, pulmonary heart disease, myocarditis, infective endocarditis, and pericarditis; control patients and patients with poor image quality due to arrhythmia were also excluded. A subset of these (104 patients with chronic MI and 10 control patients) was included in a previous preliminary study (20).

Imaging Protocol

Cardiac MRI was performed using a 3-T MRI system (Verio; Siemens, Erlangen, Germany). Retrospectively gated balanced steady-state free-precession nonenhanced cardiac cine images with 25 reconstructed phases were acquired (repetition time msec/echo time msec, 3.36/1.47; field of view, 286 × 340 mm^2; matrix, 216 × 256; average temporal resolution, ~40 msec) during repeated breath holds in short-axis views covering the whole left ventricle.

LGE MRI was performed in the same orientations and with the same section thickness using a two-dimensional segmented fast low-angle shot phase-sensitive inversion recovery sequence (4.09/1.56; field of view, 284 × 350 mm^2; matrix, 163 × 256) 10 minutes after intravenous injection of gadolinium-based contrast agent (Magnevist, 0.2 mmol/kg; Bayer Healthcare, Berlin, Germany).

Full details of both protocols are given in Appendix E1 (online).

Ground Truth Definition

Data standardization and left ventricle localization.—Images from nonenhanced cardiac cine and LGE MRI were cropped automatically into 64 × 64 pixels (pixel size, 1.46 × 1.46 mm^2), which included the full left ventricle area. Sections beyond the most base and apex regions were excluded manually.

Endocardial and epicardial contours delineation.—Endocardial and epicardial contours were manually delineated on the LGE MRI by a radiologist (N.Z., with 7 years of experience in cardiovascular MRI) after rigid registration (21) of the end-diastole phase of the cine and LGE images. Following visual inspection and assessment by mutual information, any residual registration errors were corrected using a diffeomorphic image registration technique (22) with parameterized deformation fields.

MI delineation.—MI was manually outlined on the LGE images by the same radiologist (N.Z.) after appropriate setting of the display window level and width. Microvascular obstructions were included in the MI regions.

All manual segmentations (epicardial and endocardial contours and MI) were reviewed by another expert (L.X., with 10 years of experience in cardiovascular MRI) and in cases of disagreement, a consensus was reached. The MI area percentage (23) was calculated as (MI pixels/left ventricle myocardium pixels) × 100%.

Segment model.—A 16-segment model proposed by the American Heart Association was used, in which the apex was

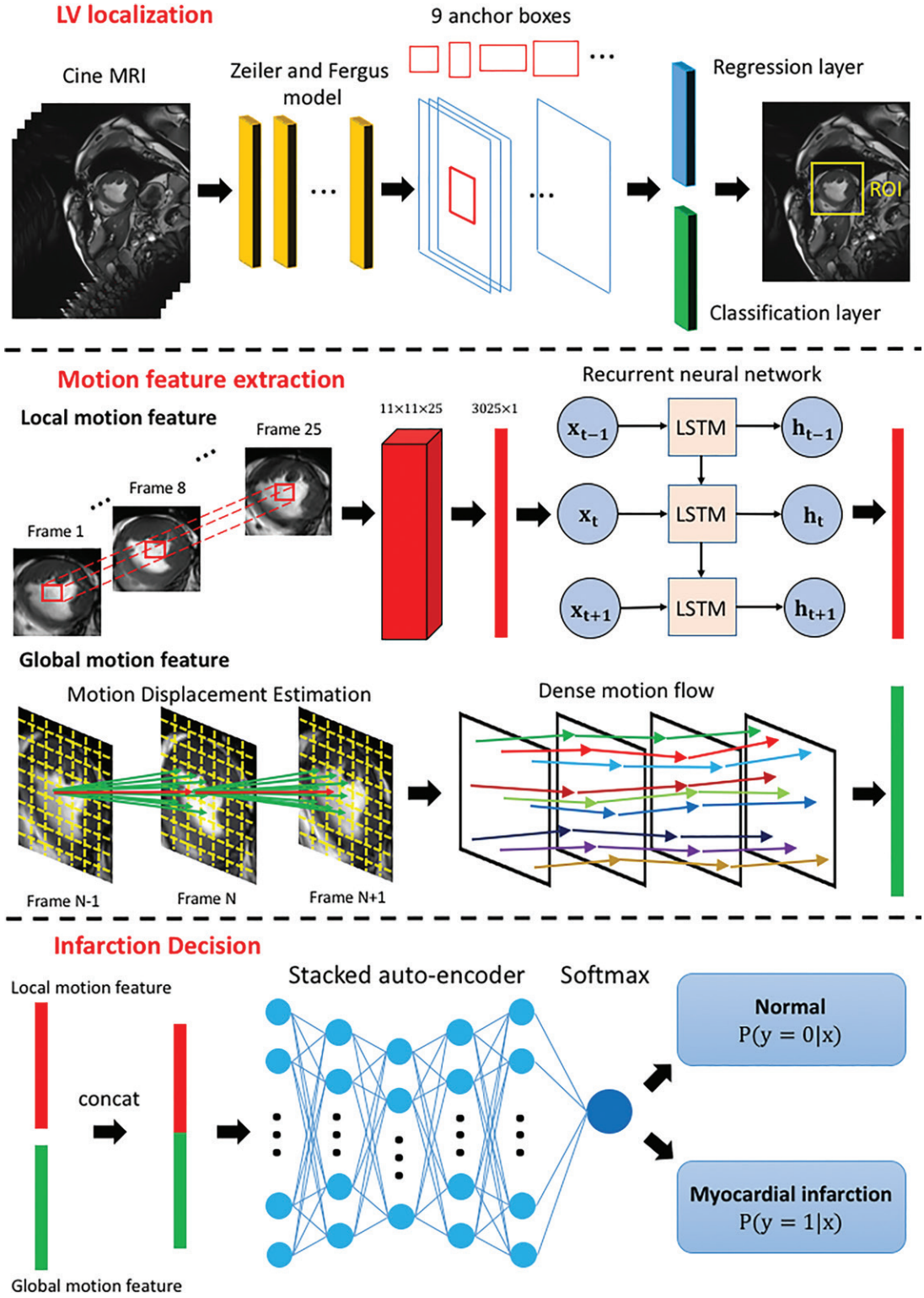

Figure 2: Major components of the proposed deep learning framework including left ventricle (LV) localization (upper panel); motion feature extraction (2D+t cine time-series input data, middle panel); and prediction and decision for the myocardial infarction (lower panel). LSTM = long short-term memory, ROI = region of interest.

excluded (24). The MI area in each segment was calculated and each segment was categorized as having no MI, transmural MI (MI area > 50% of the myocardium), or subendocardial MI (MI area ≤ 50% of the myocardium) (25).

Deep Learning

Our deep learning model extracts representative local and global motion features in nonenhanced cardiac cine MRI and relates them to LGE images (details in Appendix E1 [on-

Table 2: Quantitative Results of Diagnosis of Chronic MRI (in Independent Testing Data Sets) Using Deep Learning Framework on a Single End-Diastolic Nonenhanced Cardiac Cine Image and Full Nonenhanced Cardiac Cine Images

Method	Sensitivity (%) (*n* = 127)	Specificity (%) (*n*= 849)	AUC
Single nonenhanced cardiac cine MRI			
Overall MI segments	38.6 (49/127) [30.2, 47.7]	77.4 (657/849) [74.4, 80.1]	0.58 [0.52, 0.64]
Full nonenhanced cardiac cine MRI			
Overall MI segments	89.8 (114/127) [82.8, 94.2]	99.1 (841/849) [98.1, 99.6]	0.94 [0.91, 0.98]
Apical sections	87.1 (27/31) [69.2, 95.8]	99.1 (211/213) [96.3, 99.8]	0.96 [0.86, 1.00]
Midcavity sections	91.8 (45/49) [79.5, 97.3]	99.1 (314/317) [97.0, 99.8]	0.94 [0.91, 1.00]
Basal sections	89.4 (42/47) [76.1, 96.0]	99.1 (316/319) [97.0, 99.8]	0.93 [0.89, 0.99]
Subendocardial MI segments	81.8 (36/44) [66.8, 91.3]	99.2 (925/932) [98.4, 99.7]	0.91 [0.84, 0.97]
Apical sections	75.0 (9/12) [42.8, 93.3]	99.1 (230/232) [96.6, 99.9]	0.87 [0.72, 1.00]
Midcavity sections	81.3 (13/16) [53.7, 95.0]	99.1 (347/350) [97.3, 99.8]	0.90 [0.79, 1.00]
Basal sections	87.5 (14/16) [60.4, 97.8]	99.4 (348/350) [97.7, 99.9]	0.94 [0.84, 1.00]
Transmural MI segments	94.0 (78/83) [85.8, 97.7]	99.4 (888/893) [98.6, 99.8]	0.94 [0.90, 0.98]
Apical sections	94.7 (18/19) [71.9, 99.7]	99.6 (224/225) [97.2, 99.9]	0.95 [0.91, 1.00]
Midcavity sections	96.9 (32/33) [82.5, 99.8]	99.4 (331/333) [97.6, 99.9]	0.95 [0.90, 1.00]
Basal sections	90.3 (28/31) [73.1, 97.5]	99.4 (333/335) [97.6, 99.9]	0.93 [0.89, 1.00]

Note.—Data are percentages. Data in parentheses are raw data (number of segments or sections) used to calculate percentages. Data in brackets are 95% confidence intervals. If more than half of the pixels in a segment were MI positive, then that segment was MI positive. AUC = area under the receiver operating characteristic curve, MI = myocardial infarction.

Table 3: Calculated *P* Values between Overall Groups in Table 2

	P Value		
Groups Compared	Sensitivity	Specificity	AUC
Overall MI segments (single phase) vs overall MI segments (full 25 phases)	<.001	<.001	<.001
Overall MI segments (single phase) vs overall subendocardial MI segments (full 25 phases)	<.001	<.001	<.001
Overall MI segments (single phase) vs overall transmural MI segments (full 25 phases)	<.001	<.001	<.001
Overall MI segments (full 25 phases) vs overall subendocardial MI segments (full 25 phases)	.17	.66	.29
Overall MI segments (full 25 phases) vs overall transmural MI segments (full 25 phases)	.29	.35	.27
Overall subendocardial MI segments (full 25 phases) vs overall transmural MI segments (full 25 phases)	.03	.61	.09

Note.—Statistical differences between groups for AUC was assessed by using the Hanley & McNeil method (31). Statistical difference between groups for sensitivity and specificity was assessed by using the χ^2 test. AUC = area under the receiver operating characteristic curve, MI = myocardial infarction.

line]). Once the model is trained, predictions of MI location, size, and transmurality can be made without LGE images.

The deep learning framework consists of (Fig 2): *(a)* a localization deep network for detecting the left ventricle; *(b)* a motion feature extraction component incorporating local motion features extracted from a recurrent neural network and global motion features derived using an advanced optical flow method; and *(c)* a fully connected discriminative network (26) that distinguishes MI from normal myocardium. The deep motion networks output a probability map, and a threshold of 0.5 was used to create the final binary segmentation. The MI determined from nonenhanced cine versus from LGE MRI were compared with Dice scores (27). Analyses were performed using the full 25-phase cine data set and using a single end-diastolic frame, the latter having significant time savings.

Our implementation is open source and it is accessible at *https://github.com/xuchenchuzw/MI-Segmentation#mi-segmentation*, which has stored the version we used to achieve the current reported results.

Experimental Settings

The performance of our trained deep learning model was evaluated using independent testing, that is, a data set was not used for model development (external validation as mentioned in Park et al [28]). The 299 participants were randomly divided 80:20 into training data sets (169 patients with chronic MI, 69 control patients) and independent testing data sets (43 patients with chronic MI, 18 control patients). Basal, midcavity, and apical sections were analyzed in each participant, resulting in a total of 3808 segments for training and 976 segments for independent testing.

In addition, 10-fold cross-validation (29,30) on the whole data sets (with 299 participants) was performed to further confirm the effectiveness of our proposed deep learning model (details and secondary results are shown in Appendix E1 [online]).

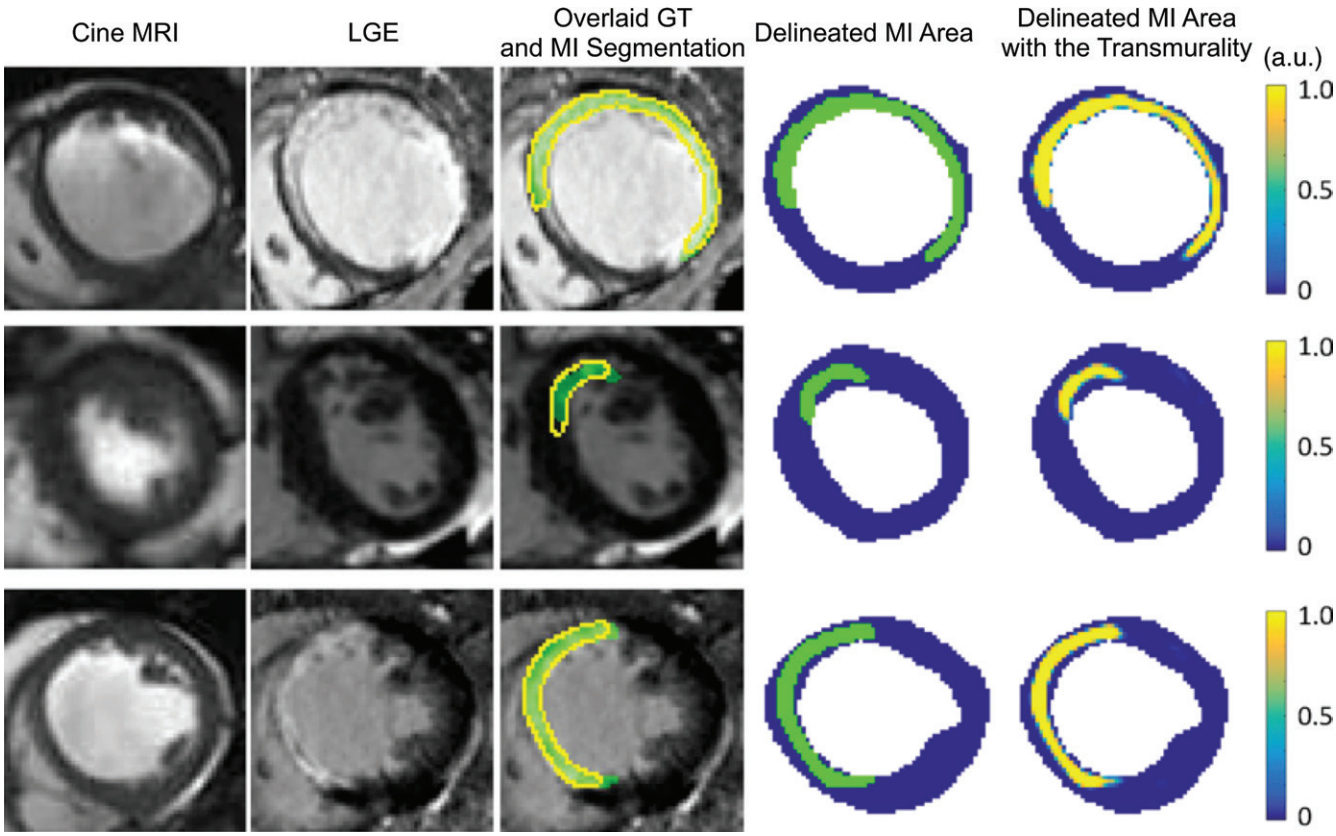

Figure 3: Each row shows data from a representative study participant. First column: Single frame from coregistered nonenhanced cardiac cine MRI. Second column: Coregistered late gadolinium enhancement (LGE) MRI. Third column: Coregistered LGE MRI with segmented myocardial infarction (MI) from nonenhanced cardiac cine images (in light green) and manually delineated ground truth (GT) from LGE images (yellow outlines) overlaid. Fourth column: Segmented MI areas (in light green) and normal left ventricle myocardium (blue). Last column: Estimated extent and transmurality (colormap shows the probabilities of the MI). a.u. = arbitrary unit.

Statistical Analysis

Statistical analysis was performed using SPSS 23.0 (SPSS, Chicago, Ill). Independent *t* tests and χ^2 tests were used to compare differences between two groups for continuous and dichotomous variables, respectively.

Using manually delineated LGE images as the ground truth, sensitivity and specificity of the delineated MI derived from nonenhanced cardiac cine images with our deep learning framework were calculated. We also performed analysis of the area under the receiver operating characteristic curve (AUC).

MI area and MI area percentage at the segmental level were normally distributed (Kolmogorov–Smirnoff test) and differences from ground truth were assessed using paired *t* testing, Pearson correlation, and Bland-Altman analyses. Differences between count variables (per segment, per section, and per patient) were assessed by using the McNemar test. A two-sided *P* value less than .05 was considered to indicate a statistically significant difference.

Results

Study Population Characteristics

No significant differences were found in weight and height between patients with chronic MI and control patients (training data sets, $P = .82$ and $P = .23$; independent testing data sets, $P = .26$ and $P = .58$). Table 1 and Table E1 (online) show that men were more common in the chronic MI cohort than in the control cohort (training data sets, 131 of 169 [77.5%] vs 33 of 69 [47.8%], respectively [$P = .001$]; independent testing data sets, 40 of 43 [93.0%] vs nine of 18 [50.0%], respectively [$P = .001$]). Patients with chronic MI were also older than control patients (Table 1) and had poorer cardiac function (eg, cardiac output: training data sets, 3.5 L/min ± 2.5 vs 4.4 L/min ± 1.4, respectively [$P = .002$]; independent testing data sets, 3.2 L/min ± 1.5 vs 4.2 L/min ± 1.2, respectively [$P = .001$]). In addition, we found that with similar weight and height, the left ventricle chamber was dilated for the patients with chronic MI (left ventricular end-diastolic volume index: training data sets, 155.3 mL/m^2 ± 89.0 vs 89.0 mL/m^2 ± 18.3, respectively [$P < .001$]; independent testing data sets, 132.6 mL/m^2 ± 68.0 vs 90.2 mL/m^2 ± 20.2, respectively [$P = .001$]).

Computational Time

The parameters of our deep learning implementation are summarized in Figure E1 (online). The training time of our deep learning on the entire 238 data sets is 373 minutes (~1.6 minutes per data set). In the test phase, the computational time is 191 seconds for one MRI data set and about 8 seconds for one MRI section.

Independent Testing on Single End-Diastolic Phase and Full Nonenhanced Cardiac Cine Images

The quantitative results of using our deep learning framework on single end-diastolic and full nonenhanced cardiac cine image data sets are summarized in Tables 2 and 3. As expected, the

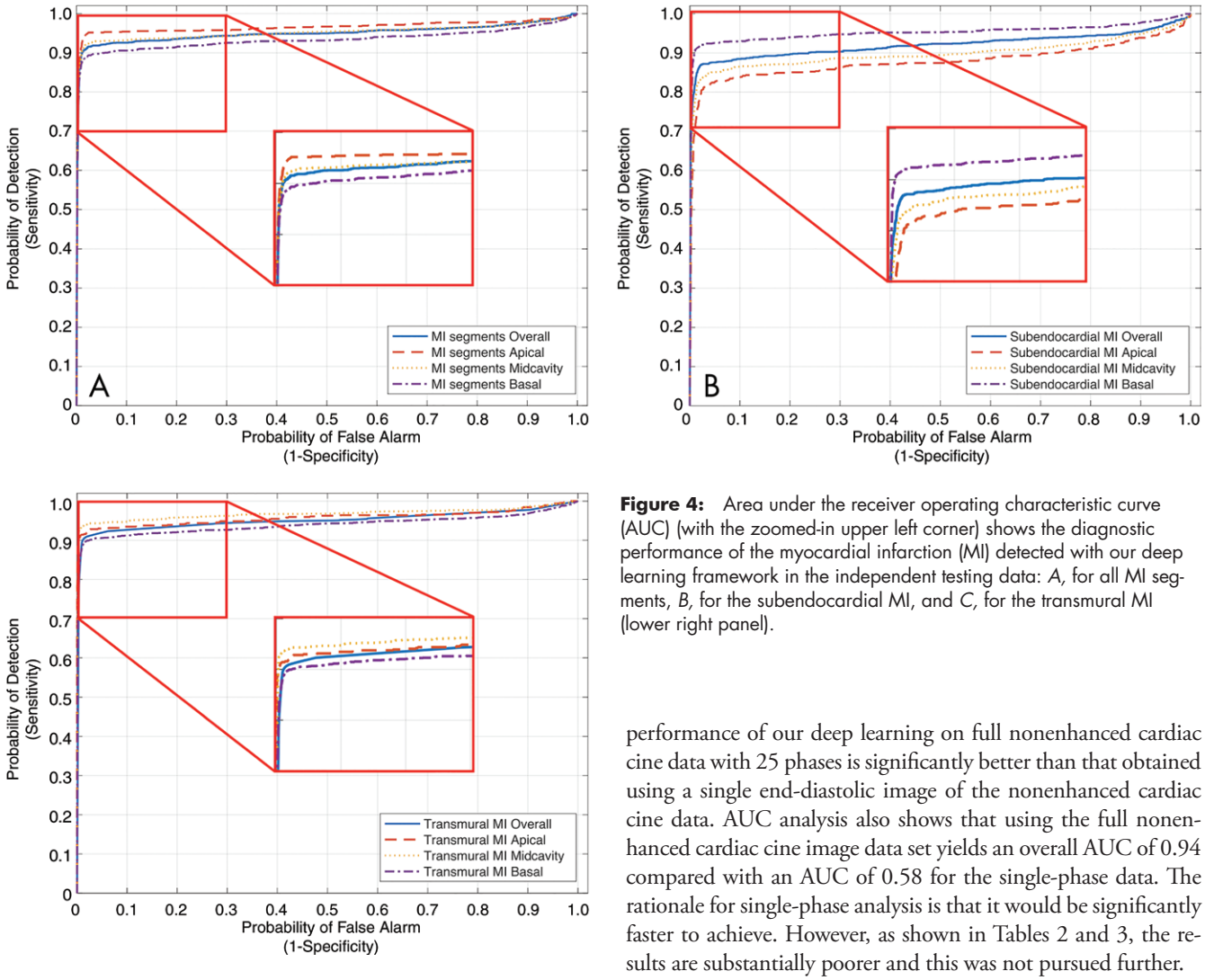

Figure 4: Area under the receiver operating characteristic curve (AUC) (with the zoomed-in upper left corner) shows the diagnostic performance of the myocardial infarction (MI) detected with our deep learning framework in the independent testing data: *A*, for all MI segments, *B*, for the subendocardial MI, and *C*, for the transmural MI (lower right panel).

Table 4: Comparison of Per-Segment Results (in Independent Testing Data Sets) for Deep Learning on Full Nonenhanced Cardiac Cine Images versus Ground Truth Delineated Manually on LGE Images

Type of MI Segment	Deep Learning	LGE	*P* Value (LGE vs Deep Learning)
Overall	114	127	.38
Apical sections	27	31	.68
Midcavity sections	45	49	1.00
Basal sections	42	47	.72
Subendocardial	36	44	1.00
Apical sections	9	12	1.00
Midcavity sections	13	16	1.00
Basal sections	14	16	1.00
Transmural	78	83	.75
Apical sections	18	19	.48
Midcavity sections	32	33	1.00
Basal sections	28	31	.69

Note.—LGE = late gadolinium enhancement, MI = myocardial infarction. Agreement of count variables was assessed by the McNemar test.

performance of our deep learning on full nonenhanced cardiac cine data with 25 phases is significantly better than that obtained using a single end-diastolic image of the nonenhanced cardiac cine data. AUC analysis also shows that using the full nonenhanced cardiac cine image data set yields an overall AUC of 0.94 compared with an AUC of 0.58 for the single-phase data. The rationale for single-phase analysis is that it would be significantly faster to achieve. However, as shown in Tables 2 and 3, the results are substantially poorer and this was not pursued further.

By using the full nonenhanced cardiac cine image data, the overall sensitivity and specificity for the detection of MI segments were almost all higher than 90%, with the exceptions being sensitivity for detection of subendocardial MI (36 of 44 [81.8%]; 95% confidence interval [CI]: 66.8%, 91.3%) and sensitivity for detection of all MI (114 of 127 [89.8%]; 95% CI: 82.8%, 94.2%). Results were similar for basal, midcavity, and apical sections. There were no MI segments found in control patients. In addition, the Dice score between the MI segmentation from nonenhanced cardiac cine MRI and the ground truth segmentation in the independent testing data sets was 86.1% ± 5.7.

Correlation with Manual Segmentation

Figure 3 shows three examples of the MI delineation results using the full nonenhanced cardiac cine image data sets compared with the manually segmented MI on LGE MRI. The MI transmurality is visualized as the predictive probabilities output from our deep learning framework, with probability greater than 0.5 being transmural and 0.5 or less being subendocardial MI. In so doing, we have a probability map to visualize the MI transmurality. Figure 4 shows AUC analyses for total, transmural, and subendocardial MI segments in basal, midcavity, and apical sections. All AUC values are 0.87

Table 5: Comparison of Per-Patient and Per-Section Results (in Independent Testing Data Set) for Deep Learning on Full Nonenhanced Cardiac Cine Images versus Ground Truth Delineated Manually on LGE Images

Metric	Deep Learning	LGE	*P* Value
Per patient			
Patients with MI			
Overall	36	43	.07
Left ventricle area (cm^2)	…	29.5 ± 15.5	…
MI area (cm^2)	6.2 ± 2.8	5.5 ± 2.3	.27
MI area percentage (%)	21.5 ± 17.3	18.5 ± 15.4	.17
Sensitivity*	36/43 (83.7) [68.7, 92.7]		…
Specificity*	17/18 (94.4) [70.6, 99.7]		…
AUC	0.89		…
Patients with subendocardial MI			
Overall	12	14	.13
Patients with transmural MI			
Overall	24	29	.22
Patients without MI			
Overall	17	18	.07
Per section			
Overall	74	88	.11
Apical	19	21	.34
Midcavity	27	34	.80
Basal	28	33	.42
Sudendocardial	21	29	.38
Apical	6	7	.61
Midcavity	7	11	.10
Basal	8	11	.72
Transmural	53	59	.23
Apical	13	14	.61
Midcavity	20	23	.72
Basal	20	22	.68

Note.—AUC = Area under the receiver operating characteristic curve, CI = confidence interval, LGE = late gadolinium enhancement, MI = myocardial infarction. MI area and MI area percentage at the segmental level were normally distributed (Kolmogorov–Smirnoff test) continuous variables, and differences from ground truth were assessed using paired *t* testing. Agreement of count variables was assessed by the McNemar test.

*Data in parentheses are percentages. Data in brackets are 95% confidence intervals.

or greater, which shows the robustness of the developed deep learning framework.

Table 4 summarizes the comparative results between our deep learning framework and LGE in the independent testing data sets (per segment) for all MIs and for transmural and subendocardial MI subgroups, with no significant differences. Table 5 summarizes the per-patient and per-section results, respectively. Ten-fold cross-validation showed very similar per-segment, per-section, and per-patient results (Tables E2 and E3 in Appendix [online]).

Pearson correlation and Bland-Altman analyses for MI area and MI area percentage are shown in Figure 5 (per-section results) with correlation coefficients of 0.94 and 0.95, respectively. The corresponding biases (limits of agreement) are −0.2 cm^2 (−0.72 cm^2, 0.32 cm^2) and −1.2% (−13%, 11%). Two example images—one with good correlation and one with poorer correlation—are also shown. Per-patient results in Figure 6 also show strong correlations of the MI area and MI area percentage (correlation coefficients, 0.88 for MI area and 0.89 for MI area percentage) measured from nonenhanced cardiac cine MRI and the manual delineated ground truth from the LGE MRI.

Discussion

In our study, we developed a fully automatic deep learning framework to detect chronic myocardial infarction (MI) in nonenhanced cardiac cine images based on extracted motion features. Using an independent testing data set, the Dice score (86.1% ± 5.7) and correlations (per-patient MI area, 6.2 cm^2 ± 2.8 vs 5.5 cm^2 ± 2.3 [P = .27; r = 0.88] and per-patient MI area percentage, 21.5% ± 17.3 vs 18.5% ± 15.4 [P = .17; r = 0.89]) between chronic MI segmented from nonenhanced cardiac cine images and that manually delineated on LGE images show that our deep learning approach is able to detect the

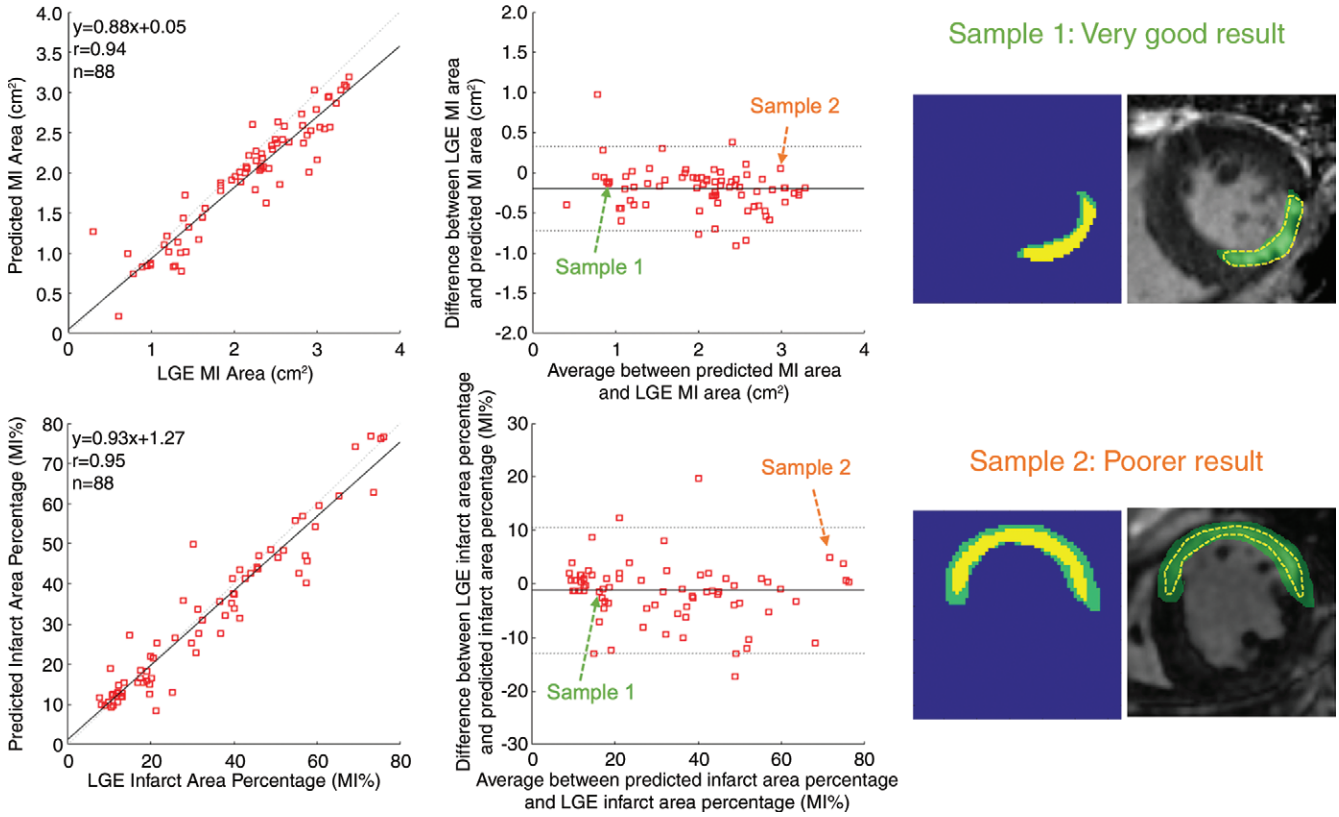

Figure 5: Pearson correlation (left) and Bland-Altman analysis (middle) of per-section analysis show that the myocardial infarction (MI) delineated by our deep learning on nonenhanced cardiac cine MRI is in accordance with the ground truth MI regions segmented on late gadolinium enhancement (LGE) MRI (independent testing data set). Segmentation results (right) are shown for a well-correlated section (Sample 1) and for a less well-correlated section (Sample 2). Dotted yellow line = ground truth manual segmentation from LGE images, green shaded region = MI detected from deep learning on nonenhanced cardiac cine images.

presence, position, transmurality, and size of chronic MI without requiring additional information from LGE images. Poorer overall sensitivity was obtained for subendocardial MIs (36 of 44 [81.8%]; 95% CI: 66.8%, 91.3%) compared with transmural MIs (78 of 83 [94.0%]; 95% CI: 85.8%, 97.7%) (P = .03), which may be attributed to their higher circumferential strain (19). The major contribution of our study is that chronic MI can be diagnosed from routinely acquired nonenhanced cardiac cine images.

Our study benefits from the fast development of deep learning techniques, which have demonstrated superior performance in medical image analysis by leveraging available big data (32,33). Previous studies have shown that some subtle changes in medical images, for example, progression of abnormality, can be distinguished with higher precision and sensitivity via deep neural networks than human visual inspection (32,33). Our study shows that myocardial wall motion may be used to accurately predict chronic MI area via deep learning. Overall, the deep learning approach achieved high sensitivity, specificity, and AUC for chronic MI detection. Compared with previous motion feature tracking methods, our framework (based on a recurrent neural network) can compress local motion distribution while extracting the global motion field from region of interest time series and generate a dense motion field to comprehensively characterize both local and global motions.

Our framework only requires nonenhanced cardiac cine images, which are routinely acquired as part of a cardiac examination for function assessment. Other approaches using nonenhanced cardiac cine MRI combined with tagging and/or feature-tracking techniques have also differentiated established or chronic MI from healthy remote myocardium. However, while Ogawa et al (19) showed that MI presence and position could be assessed using both feature tracking and myocardial tagging, the sensitivity and specificity for detecting MI segments were low (feature tracking: sensitivity, 72%; specificity, 71%; tagging technique: sensitivity, 71%; specificity, 75%). Fent et al (34) also reported that feature tracking could identify prior MI but the AUC was low (0.66 [95% CI: 0.54, 0.79], P = .012).

The feasibility of $T_{1\rho}$ cardiac MRI (35,36) for nonenhanced detection of chronic MI has also been shown but the contrast-to-noise ratio between healthy tissue and MI is low and further sequence developments are required. More recently, texture analysis has been investigated for detecting subacute and chronic MI from nonenhanced cardiac cine; sensitivity of 86% and specificity of 82% was obtained by Bessler et al (37) and overall AUC of 0.85 was achieved by Larroza et al (38).

Our study has a number of limitations: *(a)* It is a proof-of-concept study using retrospective data from a single vendor

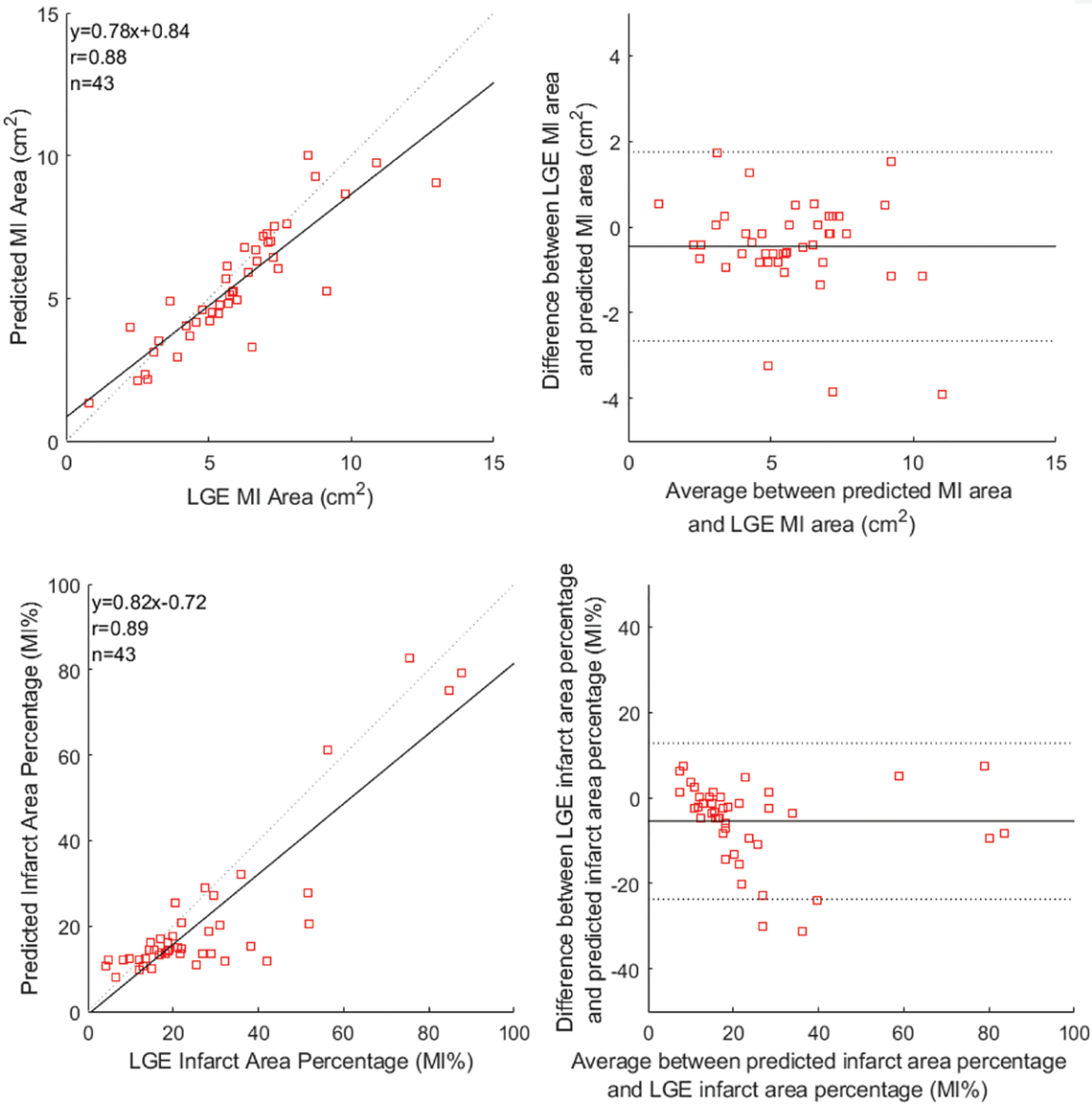

Figure 6: Pearson correlation (left) and Bland-Altman analysis (right) of per-patient analysis show that the myocardial infarction (MI) delineated by our deep learning on nonenhanced cardiac cine MRI is in accordance with the ground truth MI regions segmented on late gadolinium enhancement (LGE) MRI (independent testing data set).

and single center. *(b)* Our independent testing data set was small, consisting of 43 patients with chronic MI and 18 control patients (20% of all patients). *(c)* Our ground truth endocardium, epicardium, and MI delineations were performed manually by a single expert due to limited resources. These were then reviewed by a second expert who either ratified the first expert's segmentation or made minor modifications (by consensus following joint discussion). As such, we are unable to provide interrater agreement. It should also be noted that for our study, any microvascular obstructions were included in the MI regions, although this may affect the motion features (39). *(d)* For the single-phase method, we only tested an end-diastolic phase but an end-systolic phase may have performed better. However, this is not due to any inherent limitations in the methodology itself but reflects the fact that the LGE data that we had available to train the model was acquired in end diastole. *(e)* We have not assessed how the number of cardiac phases in the cine study affects diagnostic accuracy of the technique.

In conclusion, a robust deep learning framework for using nonenhanced cardiac cine MRI to infer the likely location, extent, and transmurality of myocardial infarction (MI) has been described, which can be readily expanded to future prospective studies. Future larger-scale studies with data from multiple sites are required for a full validation of our deep learning framework. These would also allow the accuracy of MI prediction to be determined for different myocardial segments with different motion characteristics. Further comparison with microvascular obstructions excluding data and texture analysis will be investigated in future work.

Author contributions: Guarantors of integrity of entire study, G.Y., Y.Z., L.X., H.Z.; study concepts/study design or data acquisition or data analysis/interpretation, all authors; manuscript drafting or manuscript revision for important intellectual content, all authors; approval of final version of submitted manuscript, all authors; agree to ensure any questions related to the work are appropriately resolved, all authors; literature research, G.Y., Y.Z., L.X., Z.F., D.F.; clinical studies, N.Z., Y.Z., R.S., L.X., Z.F.; experimental studies, G.Y., C.X., Y.Z., H.Z.; statistical analysis, G.Y., Z.G., C.X., Y.Z.; and manuscript editing, N.Z., G.Y., Z.G., Y.Z., J.K., L.X., H.Z., D.F.

Disclosures of Conflicts of Interest: **N.Z.** disclosed no relevant relationships. **G.Y.** Activities related to the present article: disclosed grant (PG/16/78/32402) to institution from British Heart Foundation. Activities not related to the present article: disclosed no relevant relationships. Other relationships: disclosed no relevant relationships. **Z.G.** disclosed no relevant relationships. **C.X.** disclosed no relevant relationships. **Y.Z.** disclosed no relevant relationships. **R.S.** disclosed no relevant relationships. **J.K.** disclosed no relevant relationships. **L.X.** Activities related to the present article: disclosed that study was supported in part by grants from the National Key Research and Development Program of China (2016YFC1300300) and the National Natural Science Foundation of China (No. 81641069). Activities not related to the present article: disclosed no relevant relationships. Other relationships: disclosed no relevant relationships. **H.Z.** disclosed no relevant relationships. **Z.F.** disclosed no relevant relationships. **D.F.** Activities related to the present article: disclosed no relevant relationships. Activities not related to the present article: disclosed research support to institution from Siemens. Other relationships: disclosed no relevant relationships.

References

1. Tahir E, Sinn M, Bohnen S, et al. Acute versus chronic myocardial infarction: diagnostic accuracy of quantitative native T1 and T2 mapping versus assessment of edema on standard T2-weighted cardiovascular MR images for differentiation. Radiology 2017;285(1):83–91.
2. Yusuf S, Hawken S, Ôunpuu S, et al. Effect of potentially modifiable risk factors associated with myocardial infarction in 52 countries (the INTERHEART study): case-control study. Lancet 2004;364(9438):937–952.
3. Kim HW, Farzaneh-Far A, Kim RJ. Cardiovascular magnetic resonance in patients with myocardial infarction: current and emerging applications. J Am Coll Cardiol 2009;55(1):1–16.
4. Kim RJ, Albert TSE, Wible JH, et al. Performance of delayed-enhancement magnetic resonance imaging with gadoversetamide contrast for the detection and assessment of myocardial infarction: an international, multicenter, double-blinded, randomized trial. Circulation 2008;117(5):629–637.
5. Klem I, Shah DJ, White RD, et al. Prognostic value of routine cardiac magnetic resonance assessment of left ventricular ejection fraction and myocardial damage: an international, multicenter study. Circ Cardiovasc Imaging 2011;4(6):610–619.
6. Baron N, Kachenoura N, Cluzel P, et al. Comparison of various methods for quantitative evaluation of myocardial infarct volume from magnetic resonance delayed enhancement data. Int J Cardiol 2013;167(3):739–744.
7. Fox CS, Muntner P, Chen AY, et al. Use of evidence-based therapies in short-term outcomes of ST-segment elevation myocardial infarction and non-ST-segment elevation myocardial infarction in patients with chronic kidney disease: a report from the National Cardiovascular Data Acute Coronary Treatment and Intervention Outcomes Network registry. Circulation 2010;121(3):357–365.
8. Kali A, Cokic I, Tang RLQ, et al. Determination of location, size, and transmurality of chronic myocardial infarction without exogenous contrast media by using cardiac magnetic resonance imaging at 3 T. Circ Cardiovasc Imaging 2014;7(3):471–481.
9. Ledneva E, Karie S, Launay-Vacher V, Janus N, Deray G. Renal safety of gadolinium-based contrast media in patients with chronic renal insufficiency. Radiology 2009;250(3):618–628.
10. Stojanov D, Aracki-Trenkic A, Benedeto-Stojanov D. Gadolinium deposition within the dentate nucleus and globus pallidus after repeated administrations of gadolinium-based contrast agents-current status. Neuroradiology 2016;58(5):433–441.
11. Messroghli DR, Moon JC, Ferreira VM, et al. Clinical recommendations for cardiovascular magnetic resonance mapping of T1, T2, T2* and extracellular volume: a consensus statement by the Society for Cardiovascular Magnetic Resonance (SCMR) endorsed by the European Association for Cardiovascular Imaging (EACVI). J Cardiovasc Magn Reson 2017;19(1):75. [Published correction appears in J Cardiovasc Magn Reson 2018;20(1):9.] https://doi.org/10.1186/s12968-017-0389-8.
12. Abdel-Aty H, Zagrosek A, Schulz-Menger J, et al. Delayed enhancement and T2-weighted cardiovascular magnetic resonance imaging differentiate acute from chronic myocardial infarction. Circulation 2004;109(20):2411–2416.
13. Smulders MW, Bekkers SCAM, Kim HW, Van Assche LMR, Parker MA, Kim RJ. Performance of CMR methods for differentiating acute from chronic MI. JACC Cardiovasc Imaging 2015;8(6):669–679.
14. Kim PK, Hong YJ, Im DJ, et al. Myocardial T1 and T2 mapping: techniques and clinical applications. Korean J Radiol 2017;18(1):113–131.
15. Haaf P, Garg P, Messroghli DR, Broadbent DA, Greenwood JP, Plein S. Cardiac T1 mapping and extracellular volume (ECV) in clinical practice: a comprehensive review. J Cardiovasc Magn Reson 2016;18(1):89.
16. Raman FS, Kawel-Boehm N, Gai N, et al. Modified look-locker inversion recovery T1 mapping indices: assessment of accuracy and reproducibility between magnetic resonance scanners. J Cardiovasc Magn Reson 2013;15(1):64.
17. Kawel-Boehm N, Maceira A, Valsangiacomo-Buechel ER, et al. Normal values for cardiovascular magnetic resonance in adults and children. J Cardiovasc Magn Reson 2015;17(1):29.
18. Muser D, Tioni C, Shah R, Selvanayagam JB, Nucifora G. Prevalence, correlates, and prognostic relevance of myocardial mechanical dispersion as assessed by feature-tracking cardiac magnetic resonance after a first ST-segment elevation myocardial infarction. Am J Cardiol 2017;120(4):527–533.
19. Ogawa R, Kido T, Nakamura M, et al. Diagnostic capability of feature-tracking cardiovascular magnetic resonance to detect infarcted segments: a comparison with tagged magnetic resonance and wall thickening analysis. Clin Radiol 2017;72(10):828–834.
20. Xu C, Xu L, Gao Z, et al. Direct detection of pixel-level myocardial infarction areas via a deep-learning algorithm. In: Descoteaux M, Maier-Hein L, Franz A, Jannin P, Collins D, Duchesne S, eds. Medical Image Computing and Computer Assisted Intervention − MICCAI 2017. MICCAI 2017. Lecture Notes in Computer Science, vol 10435. Cham, Switzerland: Springer, 2017; 240–249.
21. Chen H, Goela A, Garvin GJ, Li S. A parameterization of deformation fields for diffeomorphic image registration and its application to myocardial delineation. In: Jiang T, Navab N, Pluim JPW, Viergever MA, eds. Medical Image Computing and Computer-Assisted Intervention – MICCAI 2010. MICCAI 2010. Lecture Notes in Computer Science, vol 6361. Berlin, Germany: Springer, 2010; 340–348.
22. Mor-Avi V, Jenkins C, Kühl HP, et al. Real-time 3-dimensional echocardiographic quantification of left ventricular volumes: multicenter study for validation with magnetic resonance imaging and investigation of sources of error. JACC Cardiovasc Imaging 2008;1(4):413–423.
23. Protti A, Sirker A, Shah AM, Botnar R. Late gadolinium enhancement of acute myocardial infarction in mice at 7T: cine-FLASH versus inversion recovery. J Magn Reson Imaging 2010;32(4):878–886.
24. Cerqueira MD, Weissman NJ, Dilsizian V, et al. Standardized myocardial segmentation and nomenclature for tomographic imaging of the heart. A statement for healthcare professionals from the Cardiac Imaging Committee of the Council on Clinical Cardiology of the American Heart Association. Circulation 2002;105(4):539–542.
25. Kim RJ, Wu E, Rafael A, et al. The use of contrast-enhanced magnetic resonance imaging to identify reversible myocardial dysfunction. N Engl J Med 2000;343(20):1445–1453.
26. Schmidhuber J. Deep learning in neural networks: an overview. Neural Netw 2015;61:85–117.
27. Yang G, Zhuang X, Khan H, et al. Fully automatic segmentation and objective assessment of atrial scars for long-standing persistent atrial fibrillation patients using late gadolinium-enhanced MRI. Med Phys 2018;45(4):1562–1576.
28. Park SH, Han K. Methodologic guide for evaluating clinical performance and effect of artificial intelligence technology for medical diagnosis and prediction. Radiology 2018;286(3):800–809.
29. Yang G, Jones TL, Howe FA, Barrick TR. Morphometric model for discrimination between glioblastoma multiforme and solitary metastasis using three-dimensional shape analysis. Magn Reson Med 2016;75(6):2505–2516.
30. Yang G, Jones TL, Barrick TR, Howe FA. Discrimination between glioblastoma multiforme and solitary metastasis using morphological features derived from the p:q tensor decomposition of diffusion tensor imaging. NMR Biomed 2014;27(9):1103–1111.
31. Hanley JA, McNeil BJ. The meaning and use of the area under a receiver operating characteristic (ROC) curve. Radiology 1982;143(1):29–36.
32. Shen D, Wu G, Suk H-I. Deep learning in medical image analysis. Annu Rev Biomed Eng 2017;19(1):221–248.
33. Henglin M, Stein G, Hushcha PV, Snoek J, Wiltschko AB, Cheng S. Machine learning approaches in cardiovascular imaging. Circ Cardiovasc Imaging 2017;10(10):e005614.
34. Fent GJ, Garg P, Foley JRJ, et al. The utility of global longitudinal strain in the identification of prior myocardial infarction in patients with preserved left ventricular ejection fraction. Int J Cardiovasc Imaging 2017;33(10):1561–1569.
35. Witschey WR, Zsido GA, Koomalsingh K, et al. In vivo chronic myocardial infarction characterization by spin locked cardiovascular magnetic resonance. J Cardiovasc Magn Reson 2012;14(1):37.

36. van Oorschot JW, El Aidi H, Jansen of Lorkeers SJ, et al. Endogenous assessment of chronic myocardial infarction with T(1ρ)-mapping in patients. J Cardiovasc Magn Reson 2014;16(1):104.
37. Baessler B, Mannil M, Oebel S, Maintz D, Alkadhi H, Manka R. Subacute and chronic left ventricular myocardial scar: accuracy of texture analysis on nonenhanced cine MR images. Radiology 2018;286(1):103–112.
38. Larroza A, López-Lereu MP, Monmeneu JV, et al. Texture analysis of cardiac cine magnetic resonance imaging to detect nonviable segments in patients with chronic myocardial infarction. Med Phys 2018;45(4):1471–1480.
39. Everaars H, Robbers LFHJ, Götte M, et al. Strain analysis is superior to wall thickening in discriminating between infarcted myocardium with and without microvascular obstruction. Eur Radiol 2018;28(12):5171–5181.